Quantitative evaluation of neuron developmental morphology in vitro using the change-point test

Ashlee Liao
Carnegie Mellon University
Wenxin Cui
Carnegie Mellon University
Yongjie Jessica Zhang
Carnegie Mellon University
Victoria Webster-Wood (vwebster@andrew.cmu.edu)
Carnegie Mellon University

Research Article

Keywords: Neuron, Morphogenesis, Morphometrics, Change-Point Test, Developmental Growth Stages

Posted Date: April 8th, 2022

DOI: https://doi.org/10.21203/rs.3.rs-1527309/v1

Quantitative evaluation of neuron developmental morphology *in vitro* using the change-point test

Ashlee Liao [0000-0002-1828-8773][1], Wenxin Cui [0000-0002-0887-2933][1,2], Yongjie Jessica Zhang [0000-0001-7436-9757][1,2] and Victoria Webster-Wood [0000-0001-6638-2687][1,2,3*]

[1]Mechanical Engineering Department, Carnegie Mellon University, 5000 Forbes Avenue, Pittsburgh, 15213, Pennsylvania, United States of America.

[2]Biomedical Engineering Department, Carnegie Mellon University, 5000 Forbes Avenue, Pittsburgh, 15213, Pennsylvania, United States of America.

[3]McGowan Institute for Regenerative Medicine, University of Pittsburgh, 4200 Fifth Avenue, Pittsburgh, 15260, Pennsylvania, United States of America.

*Corresponding author(s). E-mail(s): vwebster@andrew.cmu.edu;
Contributing authors: ashleel@andrew.cmu.edu;
wenxincu@andrew.cmu.edu; jessicaz@andrew.cmu.edu;

Abstract

Neuron morphology gives rise to distinct axons and dendrites and plays an essential role in neuronal functionality and circuit dynamics. In rat hippocampal neurons, morphological development occurs over roughly one week *in vitro*. This development has been qualitatively described as occurring in 5 stages. Still, there is a need to quantify cell growth to monitor cell culture health, understand cell responses to sensory cues, and compare experimental results and computational growth model predictions. To address this need, embryonic rat hippocampal neurons were observed *in vitro* over six days, and their processes were quantified using both standard morphometrics (degree, number of neurites, total length, and tortuosity) and new metrics (distance between change points, relative turning angle, and the number of change points) based

on the Change-Point Test to track changes in path trajectories. Of the standard morphometrics, the total length of neurites per cell and the number of endpoints were significantly different between 0.5, 1.5, and 5 days *in vitro*, which are typically associated with Stages 2-4. Using the Change-Point Test, the number of change points and the average distance between change points per cell were also significantly different between those key time points. This work highlights key quantitative characteristics, both among common and novel morphometrics, that can describe neuron development *in vitro* and provides a foundation for analyzing directional changes in neurite growth for future studies.

Keywords: Neuron, Morphogenesis, Morphometrics, Change-Point Test, Developmental Growth Stages

Information Sharing Statement

The data set presented in this work and the code used to analyze the data are available at https://doi.org/10.5281/zenodo.6415969 and https://doi.org/10.5281/zenodo.6415474, respectively.

Acknowledgements

This material is based upon work supported by the National Science Foundation Graduate Research Fellowship Program under Grant No. DGE1745016, the Faculty Early Career Development Program under Grant No. ECCS-2044785 and the LEAP HI Program under Grant No. CMMI-1953323. The authors were also supported in part by a PITA (Pennsylvania Infrastructure Technology Alliance) grant and a PMFI (Pennsylvania Manufacturing Fellows Initiative) grant. Any opinions, findings, and conclusions or recommendations expressed in this material are those of the author(s) and do not necessarily reflect the views of the National Science Foundation.

Statements and Declarations

- **Author Contributions**
  Conceptualization: Victoria Webster-Wood, Jessica Zhang;
  Data Curation: (Lead) Ashlee Liao, (Supporting) Wenxin Cui;
  Formal Analysis: Ashlee Liao;
  Funding Acquisition: Victoria Webster-Wood, Jessica Zhang;
  Investigation: Ashlee Liao;
  Methodology: Ashlee Liao, Victoria Webster-Wood;
  Software: Ashlee Liao;
  Supervision: Victoria Webster-Wood, Jessica Zhang;
  Visualization: Ashlee Liao;
  Writing - Original Draft: Ashlee Liao;

Writing - Review & Editing: Ashlee Liao, Victoria Webster-Wood, Jessica Zhang, (Supporting) Wenxin Cui;

- **Competing Interests** The authors have no competing interests to declare that are relevant to the content of this article.

1 Introduction

Mature neurons exhibit extensive arborization of their axons and dendrites (collectively neurites) to form functional connections with neighboring cells and receive sensory signals. The distinct neuronal structure is believed to give rise to the neuron's computational abilities (Cuntz, Borst, and Segev (2007); Ferrante, Migliore, and Ascoli (2013); Kanari et al. (2018); van Elburg and van Ooyen (2010); Zomorrodi, Ferecskó, Kovács, Kröger, and Timofeev (2010)). In addition, morphological differences between neuronal cell types are thought to result in their functional differences (Khalil, Farhat, and Dłotko (2021); Krichmar, Nasuto, Scorcioni, Washington, and Ascoli (2002); Mainen and Sejnowski (1996); Schaefer, Larkum, Sakmann, and Roth (2003); Vetter, Roth, and Häusser (2001)). During the development of this crucial structure in primary neurons, several morphological changes occur in distinct stages, but their features have not been statistically compared between days or stages (Dotti, Sullivan, and Banker (1988); Powell, Rivas, Rodriguez-Boulan, and Hatten (1997); Tahirovic and Bradke (2009)).

One common model for studying neuron morphological development is the embryonic rodent hippocampal neuron (Tahirovic and Bradke (2009)). Morphogenesis of hippocampal neurons can be qualitatively described in five developmental stages occurring over seven days *in vitro* (DIV) (Figure 1): (1) within the first hour of plating, small protrusions, or lamellipodia, form along the cell periphery; (2) after around 0.5 days *in vitro* (DIV), the lamellipodia transforms into a few distinct, minor processes that form the preliminary neurites; (3) at around 1-2 DIV, one of the neurites will begin to elongate at a faster rate than the other processes and differentiate into the axon; (4) after 4 DIV, the remaining neurites will develop into dendrites and begin to elongate at a higher rate, but still slower than that of the axons; (5) after one week in culture, the neuronal processes will continue to mature by forming networks with functional synaptic connections, and the dendrites will begin to exhibit dendritic spines (Dotti et al. (1988); Kaech and Banker (2006); Tahirovic and Bradke (2009)). Previously, each stage has been qualitatively described with limited quantitative descriptions of the axonal and dendritic lengths and growth rates (Dotti et al. (1988)). However, it can be challenging to identify the stage a culture is at using only those features, particularly when transitioning between stages if the same cells within a population were not tracked over time. Nevertheless, these stages are still used as expected growth events when assessing cultures (Kaech and Banker (2006)). Neurite growth quantification is needed for consistent stage identification to monitor culture health, test intra-

and extracellular sensory cues, and compare experiments and computational models (Liao, Webster-Wood, and Zhang (2021); Qian et al. (2022)).

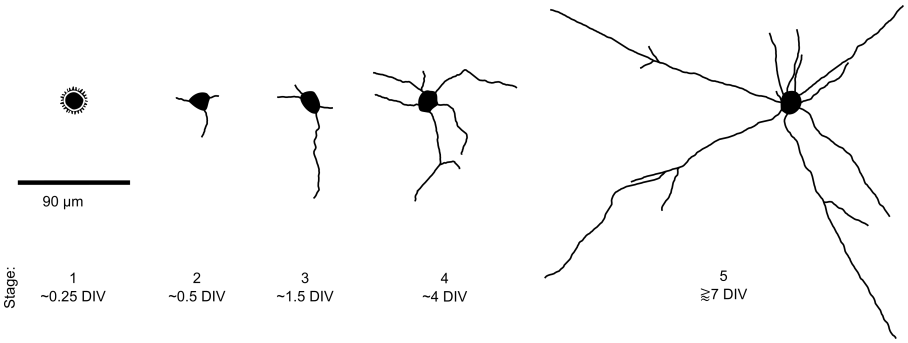

Fig. 1 Rat hippocampal neuron morphogenesis occurs in five stages (Dotti et al. (1988)). First, small protrusions, or lamellipodia, form at the soma boundary (Stage 1). Subsequently, a few lamellipodia will continue to elongate into the initial neurites (Stage 2). Next, one of the neurites will begin to grow faster than the others to differentiate into the axon (Stage 3). After a few days, the remaining neurites will also accelerate growth to mature into the dendrites (Stage 4). The final stage is the continued maturation of the entire cell, which is dependent on environmental factors and interactions with neighboring cells (Stage 5).

Many different types of quantitative representations, such as density maps (Jefferis et al. (2007); Laturnus, Kobak, and Berens (2020)), graph theory (Gillette and Grefenstette (2009); Heumann and Wittum (2009)), topology (Kanari et al. (2018)), and morphometric statistics (Laturnus et al. (2020); Polavaram, Gillette, Parekh, and Ascoli (2014); Uylings and van Pelt (2002)), have been applied to describe functionally different types of mature neurons. In addition, machine learning techniques also have been used for identifying neuron types (Laturnus et al. (2020)) and for identifying neuronal polarity (Su et al. (2021)). Laturnus et al. (2020) noted the importance of the spatial extent and shape describing neuron connectivity in distinguishing cell types, instead of specific branching features. Although these quantitative representations can characterize neuronal cell types, most have not been applied to discriminate between neurite growth stages or time points. A few common morphometrics, such as neurite length and number of branches, have been used to study neuron development *in vitro* in rat hippocampal neurons (Dotti et al. (1988)) and in stem cell differentiation to neural progenitor cells (Kang et al. (2017)). However, the current quantitative representations of neuron morphology do not capture details about changes in neurite growth direction, which can change in response to chemotropic molecules in the surrounding environment and from cell-to-cell signaling (Bicknell, Pujic, Dayan, and Goodhill (2018); Deinhardt et al. (2011); Ferreira Castro et al. (2020); Tamariz and Varela-Echavarría (2015)).

To better characterize the stages of neuron growth and quantitatively capture changes in neurite growth direction, we analyzed the development of rat

hippocampal neurons *in vitro*. Quantitative analysis was performed using both common morphometrics used to describe mature neurons and new morphometrics based on analysis using the Change-Point Test (CPT) (Byrne, Noser, Bates, and Jupp (2009); Liao et al. (2021)). The CPT was originally developed to identify locations along an animal walking path in which the direction was changed towards a resource of interest (Byrne et al. (2009)). The meandering neurite path is analogous to animal walking trajectories (Liao et al. (2021)). The trajectories can be redirected in the presence of a relevant resource, such as food for animals and growth cues in media for neurons. In addition, this test can provide additional metrics to characterize cell growth stages by including information, such as how many times the growing neurite changed direction or how long it would grow until another significant directional change.

2 Methods

2.1 Data Set Generation

A data set, comprised of images of primary rat hippocampal neurons cultured over 6 DIV and the resulting neurite traces, was created to characterize neuron morphogenesis. To generate this data set, images of *in vitro* neurons were obtained using inverted bright-field microscopy and then processed using NeuronJ (Meijering et al. (2004)) to obtain traces of the developing neurites (Figure 2) (Liao et al. (2021)).

2.1.1 Cell Culture

Cryopreserved primary, embryonic-day 18 (E18) rat hippocampal neurons (A36513, Gibco, USA) were thawed and plated in 48-well plates (150687, Nunc, USA) that were coated in poly-D-lysine (P6407, Sigma-Aldrich, USA), as per manufacturer's protocol (Thermo Fisher Scientific (2018)). Briefly, the plate was treated with 50 μg/mL poly-D-lysine (P6407, Sigma-Aldrich, USA) and incubated at room temperature for 1 hour before being rinsed with sterile, deionized water. Once dry, the plates were wrapped with Parafilm (BM999, Bemis, USA) and stored overnight in a refrigerator (2-8°C). After the wells were treated, the neurons were seeded at a density of 10,000 cells/cm^2 in Neurobasal Plus (A3582901, Gibco, USA) supplemented with 2% B-27 Plus (A3582801, Gibco, USA). The low densities allowed more neurites to be identified and traced before their arborization became too dense to distinguish individuals using bright-field microscopy. The cultures were incubated at 37°C and 5% CO_2, except during media changes and imaging periods. Twenty-four hours after initial seeding, 50% of the media was replaced with fresh media. The cultures were imaged using inverted bright-field microscopy with the Echo Revolve at 20X and 40X magnification during the following time points (DIV): 0.5, 1, 2, 3, 4, 6 (Figure 2).

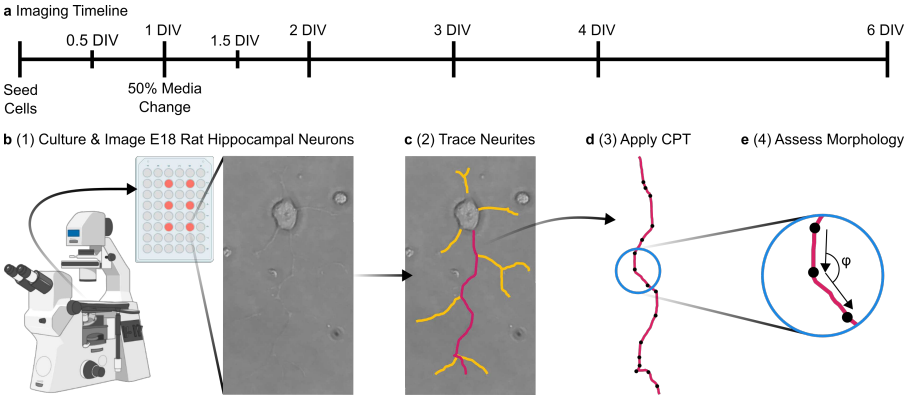

Fig. 2 There are four major steps for the methods workflow. (a-b) In the first step, cryopreserved embryonic day 18 (E18) primary rat hippocampal neurons were thawed, cultured, and monitored using inverted bright-field microscopy over six days *in vitro* (DIV) . The microscope and well plate diagram was created with BioRender.com. (c) In the second step, images of the neurites were traced using NeuronJ and then (d) quantified using the CPT. (e) Lastly, using the traces and CPT results, selected morphometrics (Figure 3) were measured and statistically analyzed using the 2-Sample Poisson Rate Test, Mann-Whitney U Test, and the 2-Sample Kolmogorov-Smirnov Test.

2.1.2 Image Processing Workflow using Semi-Automated Tracing

Neurites identified in the images were semi-automatically traced using NeuronJ (Meijering et al. (2004)), a plugin in ImageJ (Rueden et al. (2017); Schindelin et al. (2012)). All neurons included in the dataset had broad, flat somas with at least one distinct projection. This inclusion criteria ensured that the neurons had adhered to the surface of the plate and is an indication of good culture conditions (Kaech and Banker (2006)). In addition, to be included in the dataset, all of a cell's projections had to be visible within a single image, ensuring that the whole cell was captured. Overlapping neurites were excluded if their paths were not clear to prevent assigning neurites to the wrong cell or not fully tracing a neurite path. After the neurites were traced (Figure 2b), the coordinates of each neurite trace were exported out of NeuronJ as text files to be automatically evaluated for their features. In addition, metadata detailing which cell each trace belonged to were exported from NeuronJ as a comma-separated values (CSV) file.

2.2 Automatic Morphometric Evaluation of Neurite Features

After the data set was generated, the features of the developing neurites were analyzed using the CPT and quantified using both select common neuron morphometrics and novel morphometrics derived from the CPT results (Figures 2c, 2d,3). The text files detailing each neurite trace were processed using R (4.1.2) (R Core Team (2021)) within RStudio (RStudio Team (2021)). The

statistical analyses were completed using Minitab 19 (Minitab LLC (2020)), and the violin plot distributions were generated using the seaborn package (Waskom (2021)) in Python 3.7.6 (Python Core Team (2021)) using Jupyter Notebook 6.0.3 (Kluyver, Ragan-Kelley, Pérez, and Granger (2016)).

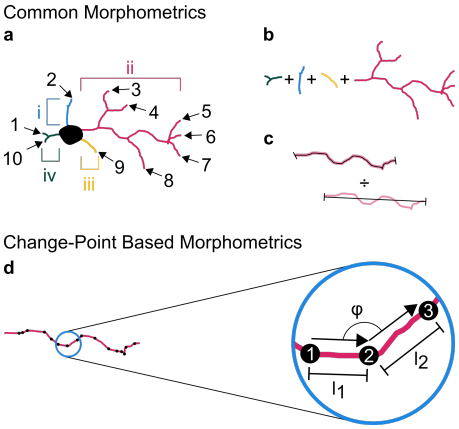

Fig. 3 Seven metrics were used to characterize neurite morphogenesis. Among the common morphometrics, there were four features: (a) degree or the number of endpoints for a given cell represented by the black arrows with Arabic numerals, number of neurites for a given cell represented by the colored brackets with Roman numerals, (b) total length of the cell or the sum of the lengths of all of its neurites, and (c) tortuosity of a neurite, which is the total path length divided by the shortest distance from its endpoints. The average tortuosity of the cell was assessed in this work. (d) In addition, a novel application of the CPT led to three new features: distance between change points indicated by l_1 and l_2, number of change points represented by the numbered black circles, and relative turning angle defined by φ.

2.2.1 Common Morphometrics

Four common morphometrics were selected to characterize neurite development (Figure 3a-c): number of neurites, degree, total length per cell, and average tortuosity per cell (Kang et al. (2017); Laturnus et al. (2020); Polavaram et al. (2014); Uylings and van Pelt (2002)). An R script was generated to calculate these features automatically based on the trace information. For each cell, degree and number of neurites were counted. The lengths of all of the neurite traces per cell were summed to calculate the total length. For each neurite trace, the length was calculated by adding the distance between consecutive coordinate points. The fourth metric, tortuosity, was calculated by taking the length of a given trace and dividing it by the distance between its two endpoint coordinates. The tortuosity was averaged for each cell.

2.2.2 Novel Morphometrics Based on a Change-Point Test

The traces were also analyzed using the CPT, which was used initially for identifying locations of significant directional changes in animal walking trajectories (Byrne et al. (2009)). The original R script presented by Byrne et al. (2009) was transformed into a callable function to process the neurite traces. Using the change points identified by the CPT, three additional neurite morphometrics were defined (Figure 3d): the number of change points, segment length, and relative turning angle. An R script was generated to automatically calculate these features based on the CPT results and the trace information. The number of change points was summed per cell as a single metric. Another metric, segment length, was defined to be the distance between two consecutive change points. Segment length was calculated by summing the distances between coordinate points between two consecutive change points. Lastly, the relative turning angle was defined as the angle measured between two consecutive segment lengths between 0°and 180°.

2.3 Statistics

Distributions of each morphometric were first tested for normality using the Anderson-Darling test. All distributions were determined to be non-normal, and therefore, non-parametric analyses were used. The continuous metrics (total length, tortuosity, segment length, and relative turning angle) at different time points were compared using the Mann-Whitney U test. Discrete metrics (degree, number of neurites, number of change points) at different time points were compared using the 2-Sample Poisson Rate test. All of the distributions were also compared using the 2-Sample Kolmogorov-Smirnov test.

3 Results

3.1 Data Set

The data set generated is comprised of three types of data (Figure 4): microscope images of neurons at seven time points, the associated traces for those neurons that met the tracing criteria (Section 2.1.2), and the resulting morphometrics (both common and new). The seven time points were selected to observe the neurons undergo three key growth stages (Figures 1 and 4): 0.5 DIV (estimated Stage 2, $n = 31$ cells, 47 traces), 1 DIV ($n = 36$ cells, 58 traces), 1.5 DIV ($n = 80$ cells, 169 traces), 2 DIV ($n = 135$ cells, 348 traces), 3 DIV ($n = 234$ cells, 830 traces), 4 DIV ($n = 162$ cells, 668 traces), and 6 DIV ($n = 20$ cells, 139 traces). This data is available at https://doi.org/10.5281/zenodo.6415474.

3.2 Common Metrics Performance

Several of the common metrics typically used for quantifying neuron morphology also showed a significant ability to discriminate between growth time

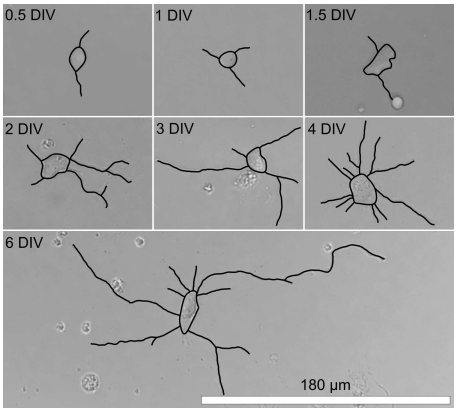

Fig. 4 Over 6 DIV, rat hippocampal neurons progress through roughly four developmental stages. The length and number of neurites and bifurcations have notable changes, which are statistically represented in Figure 7.

points. The degree and total length of all of the neurites per cell were significantly different between 20 pairs and 17 pairs out of a total of 21 pairs of time points (Figure 7), respectively, including the time points typically associated with Stages 2-4 (Figure 5). In addition, the number of neurites and average tortuosity per cell were significantly different between 14 and between 2 pairs of time points, respectively (Figure 7). The Kolmogorov-Smirnov 2-Sample test is also in general agreement with the Mann-Whitney U test and the 2-Sample Poisson Rate test.

3.3 Change-Point-Test-Based Novel Morphometrics Performance

Two of the three CPT-based morphometrics introduced in this work varied significantly between time points. The number of change points and average segment length were significantly different between 18 pairs and all 21 pairs of time points, respectively (Figure 7), including time points typically associated with Stages 2-4 (Figure 6). However, the relative turning angle was only significantly different between 1 pair of time points (Figure 7). The 2-Sample Kolmogorov-Smirnov Test results for the CPT-based morphometrics were similar to the Mann-Whitney U test and the 2-Sample Poisson Rate test (Figure 7).

4 Discussion

Our study provides a method for the quantitative description of embryonic rodent hippocampal neurons across the first week of culture through a combination of common and CPT-based morphometrics. By characterizing a sample population of cells, the morphometrics and our presented dataset can be used in the future to assess the effects of experimental conditions in combination

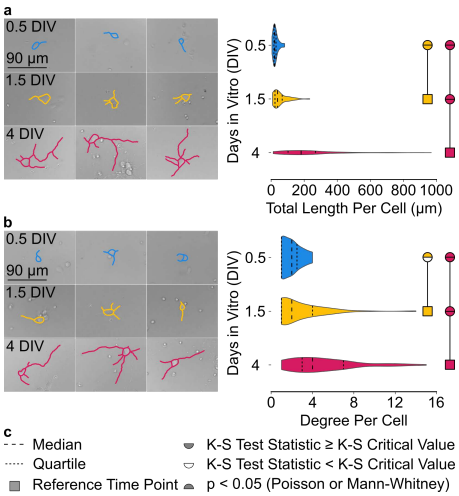

Fig. 5 Of the common morphometrics, the (a) total length per cell and the (b) degree were among the features that best distinguished between 0.5 DIV (≈ Stage 2), 1.5 DIV (≈ Stage 3), and 4 DIV (≈ Stage 4). Representative neurons are on the left panels, while the distributions are on the right. The median, upper and lower quartiles, and significance from each statistical test for each feature shown in the violin plots (a-b) are represented by the symbols in the legend (c). The Mann-Whitney U test indicated that total length was significantly different between all three time points. The 2-Sample Poisson Rate test indicated that the degree was significantly different between all three time points. The 2-Sample Kolmogorov-Smirnov test found that the distributions for degree differed significantly between 0.5 and 4 DIV and between 1.5 and 4 DIV. The distributions for total length were also significantly different for all shown time point pairs.

with the qualitative expected growth stage milestones outlined by Kaech and Banker (2006) and Dotti et al. (1988). At a population level, the distributions of total length found in our study are in alignment with the single cell values reported in Dotti et al. (1988).

When analyzing the data set at the time points associated with a specific growth stage (Figure 1), specifically 0.5 DIV (Stage 2), 1.5 DIV (Stage 3), 4 DIV (Stage 4), several features, both common and derived from the CPT, were significantly different (Figures 5-6). These differences indicate that total length, degree, segment length, and the number of change points could be used to characterize the morphological development of these neurons and possibly be used to distinguish between the associated stages. However, additional analysis would be needed to match the stages, as classified by an expert observer, with features characterized and time *in vitro*.

To quantify local changes that occur during neuron morphological development, quantitative metrics of neurite growth direction are needed. Sholl analysis (Sholl (1953)), branching angles, and tortuosity can provide a snapshot representation of the neurite spatial organization and orientation. However, they do not indicate if the difference in space or orientation is due to specific intra- or extracellular signaling or due to stochastic processes. In contrast, the CPT method (Byrne et al. (2009)) applied in the presented work

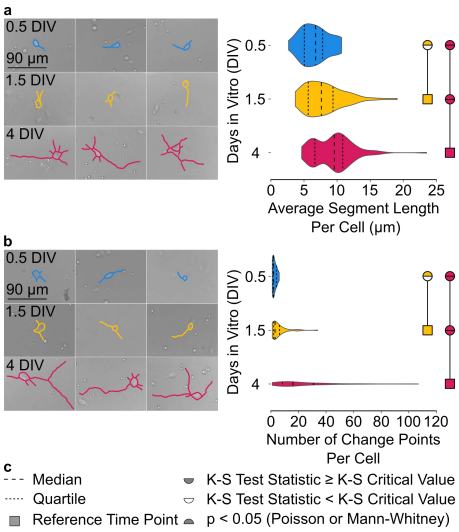

Fig. 6 From the novel CPT-Based morphometrics, the (a) average segment length and the (b) number of change points were among the features that best distinguished between 0.5 DIV (≈Stage 2), 1.5 DIV (≈Stage 3), and 4 DIV (≈Stage 4). On the left, representative neurons with traces are shown. The distributions of each feature are on the right panels. The symbols in the legend (c) represent the medians, upper and lower quartiles, and statistical significance for each feature shown in the violin plots(a-b). The Mann-Whitney U Test indicated that the average segment length was significantly different between all three time points. The 2-Sample Poisson Rate test indicated that the number of change points was significantly different between all three time points. Furthermore, the 2-Sample Kolmogorov-Smirnov test found that the distributions for both features were different between 0.5 and 4 DIV and between 1.5 and 4 DIV.

identifies where along a path in which a statistically significant directional change has occurred. From that information, the magnitude of the change and the specific angle can be extracted. The CPT was developed initially as an objective analysis of animal walking paths. Results from the CPT can be used to identify locations where the animals decided to switch from randomly meandering to being directed towards a desired resource (Byrne et al. (2009)). Analogously, the CPT could be applied in future studies to identify changes in neurite growth direction in the presence of external cues. Our study demonstrated that the CPT leads to additional morphometrics that were significantly different between key time points (Figure 6), which may indicate important directional change events during the growth stages, even in media without a controlled gradient of extracellular cues.

4.1 Limitations

This study has several limitations based on the imaging modality used for tracking the cells over time. Bright-field microscopy at 20X and 40X magnification is a method for imaging several cells over a short time-period without the potential interference of dyes that could affect the cell's structural development. Bright-field imaging can also be used to quickly assess cell health during

the culturing period. However, bright-field microscopy results in a lower contrast imaging modality than fluorescence microscopy, which is more challenging for image processing techniques to extract the neurite trajectories.

The use of the bright-field imaging technique resulted in the choice of using the semi-automatic tracing program, NeuronJ (Meijering et al. (2004)), to trace the neurites since many other automatic programs are optimized for high-contrast fluorescence images (Boulan et al. (2020); Ho et al. (2011); Kim, Son, and Palmore (2015); Pool, Thiemann, Bar-Or, and Fournier (2008)). Although the semi-automatic procedure may introduce some interobserver variability, the process will still be more reproducible than a fully manual method (Meijering et al. (2004)). Furthermore, due to the need for user input, the labor intensiveness of this method scales with the number of neurites. However, it is still an improvement over a completely manual method with better neurite centerline representations and negligible differences in length results (Meijering et al. (2004)).

In addition, without the use of fluorescence dyes, neurons cultured beyond 6 DIV become difficult to distinguish due to the development of long neurites and dense networks at Stage 5 (Kaech and Banker (2006)). Furthermore, a distinct qualitative morphological change is not present between Stage 4 and 5, and Stage 5 is likely highly influenced by other cell interactions, unlike the previous stages that are considered endogenously determined (Dotti et al. (1988)). Thus, Stage 5 was not considered as part of the scope of the work presented here. Additional studies controlling the cell interactions between developing neurons would be required to characterize Stage 5 morphology based on environmental conditions using our collection of quantitative morphometrics.

5 Conclusions

This study provided a semi-automated quantitative analysis method, including both common and novel morphometrics. We used this method to analyze growth during the initial 6 DIV for cultured neurons, which correspond to three of the five growth stages qualitatively described for embryonic rodent hippocampal neurons in culture. This semi-automated quantitative analysis method has many potential applications, including assessing the cell culture health and how certain intrinsic or extrinsic factors may alter neuron morphological development. The novel application of the Change-Point Test, which was initially developed for studying animal walking paths, could also provide additional insight on factors that alter the neurite trajectories in future studies. In addition, quantifying the development of neuron morphology can inform parameters needed for computational simulations of neuron growth (Qian et al. (2022)), materials transport (Li, Barati Farimani, and Zhang (2021); Li, Chai, Yang, and Zhang (2019)), and molecular traffic jams (Li and Zhang (2022a, 2022b)). More accurate computational models could help guide future *in vitro* studies by exploring experimental parameters *in silico* prior to costly

and time intensive experimentation. Finally, with our semi-automatic quantitative method for characterizing neuron morphology, experimental results can be consistently assessed by both novices and experts, and results can be easily compared across studies.

Appendix A: Distributions and Analyses on All Morphometrics for All Observed Time Points

Three statistical analyses were used to compare the samples of each feature at each time point (Figure 7). First, the distributions of all features at each time point were pairwise compared using the 2-Sample Kolmogorov-Smirnov (K-S) test to determine whether the samples came from different distributions. The continuous features (average segment length, average turning angle, total length, average tortuosity) were also compared using the Mann-Whitney U test, which analyzes the medians between each pair. Finally, the discrete count features (total change points, number of neurites, degree) were compared using the 2-Sample Poisson Rate test. All of the tests indicated significant differences between several time points for many of the features (Figure 7). However, the average turning angle and average tortuosity were not significantly different for most of the time points (Figures 7b and 7f).

References

Bicknell, B.A., Pujic, Z., Dayan, P., Goodhill, G.J. (2018, 6). Control of neurite growth and guidance by an inhibitory cell-body signal. *PLOS Computational Biology*, *14*(6), e1006218. Retrieved from https://doi.org/10.1371/journal.pcbi.1006218

Boulan, B., Beghin, A., Ravanello, C., Deloulme, J.-C., Gory-Fauré, S., Andrieux, A., ... Denarier, E. (2020, 7). AutoNeuriteJ: An ImageJ plugin for measurement and classification of neuritic extensions. *PLOS ONE*, *15*(7), e0234529. Retrieved from https://doi.org/10.1371/journal.pone.0234529

Byrne, R.W., Noser, R., Bates, L.A., Jupp, P.E. (2009). How did they get here from there? Detecting changes of direction in terrestrial ranging. *Animal Behaviour*, *77*(3), 619–631. Retrieved from https://doi.org/10.1016/j.anbehav.2008.11.014

Cuntz, H., Borst, A., Segev, I. (2007, 12). Optimization principles of dendritic structure. *Theoretical Biology and Medical Modelling*, *4*(1), 21. Retrieved from https://doi.org/10.1186/1742-4682-4-21

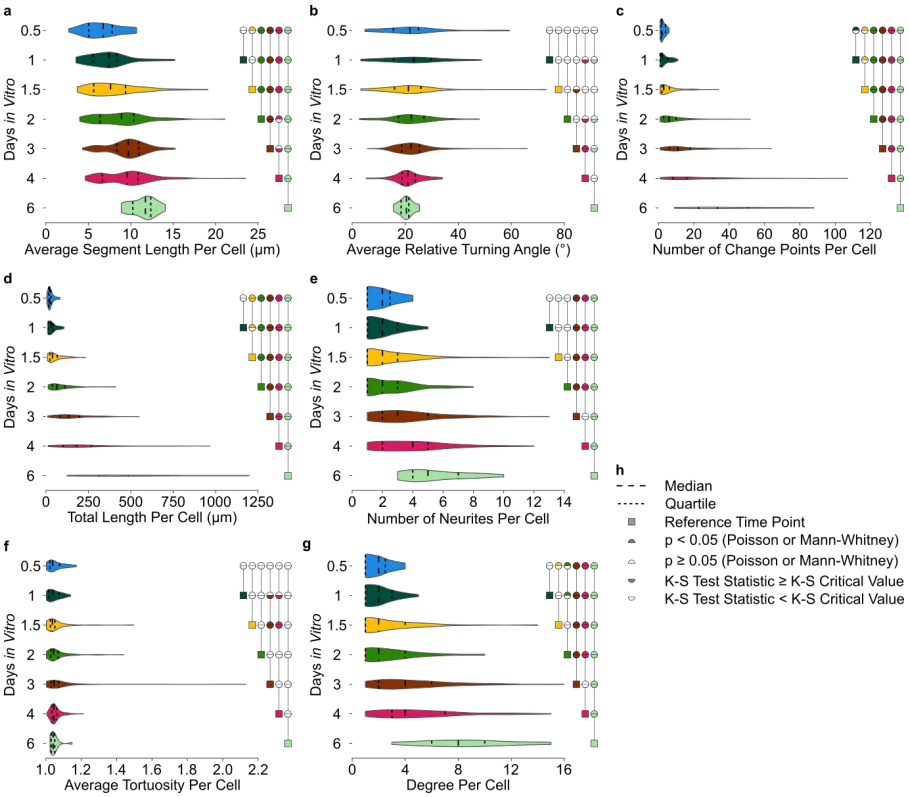

Fig. 7 The results of three statistical analyses used to assess each morphometric (CPT-Based: (a) average segment length, (b) average relative turning angle, (c) number of change points; Common: (d) total length, (e) number of neurites, (f) average tortuosity, (g) degree) for every time point pair are symbolically represented, as defined in (h).

Deinhardt, K., Kim, T., Spellman, D.S., Mains, R.E., Eipper, B.A., Neubert, T.A., ... Hempstead, B.L. (2011, 12). Neuronal growth cone retraction relies on proneurotrophin receptor signaling through Rac. *Science Signaling*, *4*(202), ra82. Retrieved from https://doi.org/10.1126/scisignal.2002060

Dotti, C.G., Sullivan, C.A., Banker, G.A. (1988, 4). The establishment of polarity by hippocampal neurons in culture. *Journal of Neuroscience*, *8*(4), 1454–1468. Retrieved from https://doi.org/10.1523/jneurosci.08-04-01454.1988

Ferrante, M., Migliore, M., Ascoli, G.A. (2013, 1). Functional impact of dendritic branch-point morphology. *Journal of Neuroscience*, *33*(5), 2156–2165. Retrieved from https://doi.org/10.1523/JNEUROSCI.3495-12.2013

Ferreira Castro, A., Baltruschat, L., Stürner, T., Bahrami, A., Jedlicka, P., Tavosanis, G., Cuntz, H. (2020, 11). Achieving functional neuronal dendrite structure through sequential stochastic growth and retraction. *eLife*, *9*. Retrieved from https://doi.org/10.7554/eLife.60920

Gillette, T.A., & Grefenstette, J.J. (2009, 9). On comparing neuronal morphologies with the constrained tree-edit-distance. *Neuroinformatics*, *7*(3), 191–4. Retrieved from https://doi.org/10.1007/s12021-009-9053-2

Heumann, H., & Wittum, G. (2009, 9). The tree-edit-distance, a measure for quantifying neuronal morphology. *Neuroinformatics*, *7*(3), 179–90. Retrieved from https://doi.org/10.1007/s12021-009-9051-4

Ho, S.-Y., Chao, C.-Y., Huang, H.-L., Chiu, T.-W., Charoenkwan, P., Hwang, E. (2011, 12). NeurphologyJ: An automatic neuronal morphology quantification method and its application in pharmacological discovery. *BMC Bioinformatics*, *12*(1), 230. Retrieved from https://doi.org/10.1186/1471-2105-12-230

Jefferis, G.S., Potter, C.J., Chan, A.M., Marin, E.C., Rohlfing, T., Maurer, C.R., Luo, L. (2007, 3). Comprehensive maps of Drosophila higher olfactory centers: Spatially segregated fruit and pheromone representation. *Cell*, *128*(6), 1187–1203. Retrieved from https://doi.org/10.1016/j.cell.2007.01.040

Kaech, S., & Banker, G. (2006, 12). Culturing hippocampal neurons. *Nature Protocols*, *1*(5), 2406–2415. Retrieved from https://doi.org/10.1038/nprot.2006.356

Kanari, L., Dłotko, P., Scolamiero, M., Levi, R., Shillcock, J., Hess, K., Markram, H. (2018). A topological representation of branching neuronal morphologies. *Neuroinformatics*, *16*(1), 3–13. Retrieved from https://doi.org/10.1007/s12021-017-9341-1

Kang, S., Chen, X., Gong, S., Yu, P., Yau, S., Su, Z., ... Shi, L. (2017, 12). Characteristic analyses of a neural differentiation model from iPSC-derived neuron according to morphology, physiology, and global gene expression pattern. *Scientific Reports*, *7*(1), 12233. Retrieved from

https://doi.org/10.1038/s41598-017-12452-x

Khalil, R., Farhat, A., Dłotko, P. (2021, 5). Developmental changes in pyramidal cell morphology in multiple visual cortical areas using cluster analysis. *Frontiers in Computational Neuroscience*, *15*, 667696. Retrieved from https://doi.org/10.3389/fncom.2021.667696

Kim, K.-M., Son, K., Palmore, G.T.R. (2015, 12). Neuron image analyzer: Automated and accurate extraction of neuronal data from low quality images. *Scientific Reports*, *5*(1), 17062. Retrieved from https://doi.org/10.1038/srep17062

Kluyver, T., Ragan-Kelley, B., Pérez, F., Granger, B. (2016). Jupyter Notebooks – a publishing format for reproducible computational workflows. F. Loizides & B. Schmidt (Eds.), *Positioning and power in academic publishing: Players, agents and agendas* (pp. 87–90). IOS Press.

Krichmar, J.L., Nasuto, S.J., Scorcioni, R., Washington, S.D., Ascoli, G.A. (2002, 6). Effects of dendritic morphology on CA3 pyramidal cell electrophysiology: A simulation study. *Brain Research*, *941*(1-2), 11–28. Retrieved from https://doi.org/10.1016/S0006-8993(02)02488-5

Laturnus, S., Kobak, D., Berens, P. (2020, 10). A systematic evaluation of interneuron morphology representations for cell type discrimination. *Neuroinformatics*, *18*(4), 591–609. Retrieved from https://doi.org/10.1007/s12021-020-09461-z

Li, A., Barati Farimani, A., Zhang, Y.J. (2021, 12). Deep learning of material transport in complex neurite networks. *Scientific Reports*, *11*(1), 11280. Retrieved from https://doi.org/10.1038/s41598-021-90724-3

Li, A., Chai, X., Yang, G., Zhang, Y.J. (2019). An isogeometric analysis computational platform for material transport simulation in complex neurite networks. *Molecular & Cellular Biomechanics*, *16*(2), 123–140. Retrieved from https://doi.org/10.32604/mcb.2019.06479

Li, A., & Zhang, Y.J. (2022a, 3). Modeling intracellular transport and traffic jam in 3D neurons using PDE-constrained optimization. *Journal of Mechanics*, *38*, 44–59. Retrieved from https://doi.org/10.1093/jom/ufac007

Li, A., & Zhang, Y.J. (2022b, 12). Modeling material transport regulation and traffic jam in neurons using PDE-constrained optimization. *Scientific Reports*, *12*(1), 3902. Retrieved from https://doi.org/10.1038/s41598-022-07861-6

Liao, A.S., Webster-Wood, V.A., Zhang, Y.J. (2021). Quantification of neuron morphological development using the change-point test. *2021 summer biomechanics, bioengineering and biotransport conference.*

Mainen, Z.F., & Sejnowski, T.J. (1996, 7). Influence of dendritic structure on firing pattern in model neocortical neurons. *Nature*, *382*(6589), 363–366. Retrieved from https://doi.org/10.1038/382363a0

Meijering, E., Jacob, M., Sarria, J.-C., Steiner, P., Hirling, H., Unser, M. (2004, 4). Design and validation of a tool for neurite tracing and analysis in fluorescence microscopy images. *Cytometry*, *58A*(2), 167–176. Retrieved from https://doi.org/10.1002/cyto.a.20022

Minitab LLC (2020). *Minitab 19 Statistical Software.* State College, PA: Minitab. Retrieved from www.minitab.com

Polavaram, S., Gillette, T.A., Parekh, R., Ascoli, G.A. (2014, 12). Statistical analysis and data mining of digital reconstructions of dendritic morphologies. *Frontiers in Neuroanatomy*, *8*, 138. Retrieved from https://doi.org/10.3389/fnana.2014.00138

Pool, M., Thiemann, J., Bar-Or, A., Fournier, A.E. (2008, 2). NeuriteTracer: A novel ImageJ plugin for automated quantification of neurite outgrowth. *Journal of Neuroscience Methods*, *168*(1), 134–139. Retrieved from https://doi.org/10.1016/J.JNEUMETH.2007.08.029

Powell, S.K., Rivas, R.J., Rodriguez-Boulan, E., Hatten, M.E. (1997, 2). Development of polarity in cerebellar granule neurons. *Journal of Neurobiology*, *32*(2), 223–236. Retrieved from https://doi.org/10.1002/(SICI)1097-4695(199702)32:2⟨223::AID-NEU7⟩3.0.CO;2-A

Python Core Team (2021). *Python: A Dynamic, Open Source Programming Language.* Python Software Foundation. Retrieved from https://www.python.org/

Qian, K., Pawar, A., Liao, A., Anitescu, C., Webster-Wood, V., Feinberg, A., ... Zhang, Y.J. (2022). Modeling neuron growth using isogeometric collocation based phase field method. *Scientific Reports*, *Under Review*.

R Core Team (2021). *R: A Language and Environment for Statistical Computing*. Vienna, Austria: R Foundation for Statistical Computing. Retrieved from https://www.R-project.org/

RStudio Team (2021). *RStudio: Integrated Development Environment for R*. Boston, MA: RStudio, PBC. Retrieved from http://www.rstudio.com/

Rueden, C.T., Schindelin, J., Hiner, M.C., DeZonia, B.E., Walter, A.E., Arena, E.T., Eliceiri, K.W. (2017, 12). ImageJ2: ImageJ for the next generation of scientific image data. *BMC Bioinformatics*, *18*(1), 529. Retrieved from https://doi.org/10.1186/s12859-017-1934-z

Schaefer, A.T., Larkum, M.E., Sakmann, B., Roth, A. (2003, 6). Coincidence detection in pyramidal neurons is tuned by their dendritic branching pattern. *Journal of Neurophysiology*, *89*(6), 3143–3154. Retrieved from https://doi.org/10.1152/jn.00046.2003

Schindelin, J., Arganda-Carreras, I., Frise, E., Kaynig, V., Longair, M., Pietzsch, T., ... Cardona, A. (2012, 7). Fiji: An open-source platform for biological-image analysis. *Nature Methods*, *9*(7), 676–682. Retrieved from https://doi.org/10.1038/nmeth.2019

Sholl, D.A. (1953, 10). Dendritic organization in the neurons of the visual and motor cortices of the cat. *Journal of anatomy*, *87*(4), 387–406.

Su, C.-Z., Chou, K.-T., Huang, H.-P., Li, C.-J., Charng, C.-C., Lo, C.-C., Wang, D.-W. (2021, 10). Identification of neuronal polarity by node-based machine learning. *Neuroinformatics*, *19*(4), 669–684. Retrieved from https://doi.org/10.1007/s12021-021-09513-y

Tahirovic, S., & Bradke, F. (2009, 9). Neuronal polarity. *Cold Spring Harbor Perspectives in Biology*, *1*(3), a001644-a001644. Retrieved from https://doi.org/10.1101/cshperspect.a001644

Tamariz, E., & Varela-Echavarría, A. (2015, 5). The discovery of the growth cone and its influence on the study of axon guidance. *Frontiers in Neuroanatomy*, *9*, 51. Retrieved from https://doi.org/10.3389/fnana.2015.00051

Thermo Fisher Scientific (2018). *B-27 Plus Neuronal Culture System.* Life Technologies. Retrieved from https://www.thermofisher.com/document-connect/document-connect.html?url=https://assets.thermofisher.com/TFS-Assets/LSG/manuals/MAN0017319_B27_PlusNeuronalCultureSystem_UG.pdf

Uylings, H.B.M., & van Pelt, J. (2002, 1). Measures for quantifying dendritic arborizations. *Network: Computation in Neural Systems*, *13*(3), 397–414. Retrieved from https://doi.org/10.1088/0954-898X_13_3_309

van Elburg, R.A.J., & van Ooyen, A. (2010, 5). Impact of dendritic size and dendritic topology on burst firing in pyramidal cells. *PLoS Computational Biology*, *6*(5), e1000781. Retrieved from https://doi.org/10.1371/journal.pcbi.1000781

Vetter, P., Roth, A., Häusser, M. (2001, 2). Propagation of action potentials in dendrites depends on dendritic morphology. *Journal of Neurophysiology*, *85*(2), 926–937. Retrieved from https://doi.org/10.1152/jn.2001.85.2.926

Waskom, M. (2021, 4). Seaborn: Statistical data visualization. *Journal of Open Source Software*, *6*(60), 3021. Retrieved from https://doi.org/10.21105/joss.03021

Zomorrodi, R., Ferecskó, A.S., Kovács, K., Kröger, H., Timofeev, I. (2010, 5). Analysis of morphological features of thalamocortical neurons from the ventroposterolateral nucleus of the cat. *The Journal of Comparative Neurology*, *518*(17), 3541–3556. Retrieved from https://doi.org/10.1002/cne.22413

Supplementary Files

This is a list of supplementary files associated with this preprint. Click to download.

- LiaoQuantitativeEvaluationOfNeuronDevelopmentalMorphologyInVitroUs.zip